

# 1 **PLA-Derived Lactate Esters as Plasma Precursors for Hydrophilic and Antibacterial** 2 **Coatings**

3  
4 Monika Strašáková<sup>1</sup>, Eva Domincová Bergerová<sup>1\*</sup>, Marián Lehocký<sup>1</sup>, Veronika Hanuliak<sup>1</sup>,  
5 Hana Pištěková<sup>1</sup>, Michal Urbánek<sup>1</sup>, Pavel St'ahel<sup>2</sup>, Monika Stupavská<sup>2</sup>, Jakub Klaban<sup>1</sup>, Anežka  
6 Lengálová<sup>3</sup>, Vladimír Sedlařík<sup>1</sup>

7 <sup>1</sup>Centre of Polymer Systems, Tomas Bata University in Zlin, tr. Tomase Bati 5678, 760 01  
8 Zlin, Czech Republic

9 <sup>2</sup> Department of Plasma Physics and Technology, Faculty of Science, Masaryk University,  
10 Kotlarska 267/2, 611 37 Brno, Czech Republic

11 <sup>3</sup> Faculty of Humanities, Tomas Bata University in Zlin, Stefanikova 5670, 760 01 Zlin,  
12 Czech Republic

13 \*Correspondence: Eva Domincová Bergerová, [domincova.bergerova@utb.cz](mailto:domincova.bergerova@utb.cz)

## 14 **Abstract**

15 This study introduces a novel concept of using lactate esters as unconventional, bio-based  
16 precursors for plasma-assisted deposition of multifunctional coatings. Unlike traditional  
17 plasma precursors, simple molecules such as methyl and ethyl lactate enable simultaneous  
18 enhancement of surface hydrophilicity and antibacterial activity on PET substrate. This work  
19 highlights a new pathway for designing advanced functional coatings using readily available  
20 ester-based compounds. Plasma deposition induced pronounced changes in surface chemistry  
21 and morphology through fragmentation–recombination mechanisms, leading to a significant  
22 increase in hydrophilicity, with the water contact angle decreasing from 76° to 27° for ethyl  
23 lactate and to 51° for methyl lactate. X-ray photoelectron spectroscopy confirmed the  
24 formation of oxygen- and nitrogen-containing functional groups, while the modified surfaces  
25 exhibited strong antibacterial performance, achieving up to 3.4 log reduction against  
26 *Escherichia coli* and 2.3 log reduction against *Staphylococcus aureus* (ISO 22196:2011).  
27 Crucially, this work establishes lactate esters as a new and versatile class of plasma  
28 precursors, demonstrating that waste-derived, low-molecular-weight compounds can  
29 outperform conventional systems in simultaneously imparting hydrophilicity and

30 antimicrobial functionality, thereby redefining their role in plasma processing and providing a  
31 scalable platform for multifunctional coatings within a circular economy framework.

32 **Keywords:** Plasma deposition, surface modification, antibacterial properties, polylactic acid  
33 ester, polymeric material

34

## 35 **1. Introduction**

36 Plastics have become some of the most widely produced and utilized materials globally. The  
37 substantial growth in production and consumption has led to the accumulation of large  
38 quantities of waste, presenting a significant challenge for environmentally responsible  
39 disposal. Projections suggest that annual global production will result in approximately  
40 12,000 Mt of waste by 2050. As production continues to rise, the resulting excess waste poses  
41 an increasing environmental threat to both humanity and the planet. Traditional waste  
42 management methods, such as landfilling, are inadequate due to the non-biodegradable nature  
43 of many conventional polymers, which leads to their prolonged persistence in disposal sites  
44 [1,2].

45 In response to this issue, there has been growing interest in alternative materials that retain the  
46 functional properties of conventional materials while being more environmentally sustainable.  
47 This has spurred the development of biodegradable polymers, now used in the production of  
48 eco-friendly alternatives. Bio-based polymers, aligned with the principles of sustainable  
49 production and consumption, have emerged as key materials in this context [1,3]. The demand  
50 for bioplastics has surged as a viable alternative to traditional polymers, primarily due to their  
51 renewable nature, non-toxicity, biodegradability, and biocompatibility. Furthermore, modern  
52 bio-based materials exhibit mechanical properties that are comparable to those of their fossil-  
53 derived counterparts [4].

54 Among the various bioplastics, polylactic acid (PLA) is considered one of the most promising  
55 candidates for replacing non-degradable polymers such as polyethylene terephthalate (PET)  
56 and polystyrene (PS), particularly in food packaging applications. However, the increasing  
57 production and use of PLA, combined with inadequate consumer waste collection systems  
58 and limited technological solutions for its effective recycling, have resulted in frequent cross-  
59 contamination of recycling streams. In practice, PLA waste is often unintentionally mixed  
60 with conventional plastic waste, most notably with PET recycling streams, where even small

61 amounts of PLA can negatively affect the recycling process and the quality of recycled PET.  
62 Consequently, the simultaneous management of biodegradable and non-biodegradable plastics  
63 within the same waste management infrastructure remains a significant challenge [5,6].

64 A promising approach to this issue is processing waste of these materials, which involves a  
65 systematic technological approach and the repurposing of waste. For PLA, potential  
66 processing waste routes include landfilling or composting, incineration, and both mechanical  
67 and chemical recycling. However, these methods pose several challenges, including the loss  
68 of valuable polyhydroxy acids, degradation of soil quality, and the release of toxic exhaust  
69 gases.

70 In contrast, chemical recycling represents a promising strategy for extending the lifecycle of  
71 post-consumer plastic waste. In the case of PLA, chemical recycling is considered an  
72 economically viable and environmentally sustainable approach, as it enables the  
73 depolymerization of the ester backbone into valuable low-molecular-weight compounds,  
74 primarily lactate esters, which can be further utilized as functional precursors in various  
75 applications [3]. An important advancement in surface engineering is plasma polymerization,  
76 a process in which reactive species generated in the plasma phase - such as radicals, ions, and  
77 excited molecules - are formed from a gaseous precursor and subsequently deposited onto a  
78 substrate, where they recombine to form a highly cross-linked polymer-like thin film [7].  
79 Plasma-based technologies offer several advantages, including solvent-free processing, low  
80 thermal load, and reduced use of hazardous chemicals. Importantly, plasma treatment  
81 modifies only the surface of a material while preserving its bulk properties. In addition,  
82 plasma exposure can introduce polar functional groups, such as hydroxyl and carboxyl  
83 moieties, which significantly enhance surface wettability, as evidenced by the reduction in  
84 water contact angle following treatment [8].

85 However, further research is needed on the plasma processing of PLA esters, such as ethyl  
86 lactate and methyl lactate, which are decomposition products resulting from chemical  
87 recycling. Furthermore, existing literature largely focuses on the combination of  
88 commercially available ethyl lactate with additives, nanoparticles, or composites, rather than  
89 exploring plasma deposition or polymerization of PLA decomposition products [9–11].

90 This study investigates the application of plasma technology in the processing of products  
91 derived from the chemical recycling of biopolymers, with a focus on optimizing ecological  
92 sustainability. By integrating these approaches, this work not only offers a sustainable

93 solution for addressing the projected accumulation of plastic waste by 2050 but also produces  
94 materials with enhanced properties suitable for a wide range of applications, marking a  
95 significant step forward in the implementation of circular economy practices and the  
96 development of sustainable materials.

97 Considering the need for more sustainable valorization routes for chemically recycled PLA  
98 monomers and the scarcity of studies on their plasma-assisted deposition, there is a clear  
99 research gap. Moreover, PET is one of the most common non-biodegradable packaging  
100 materials and provides an ideal substrate for surface modification, where tailored coatings can  
101 impart new functionalities without altering bulk properties.

102 Therefore, the aim of this study is to investigate the plasma-assisted deposition of methyl  
103 lactate and ethyl lactate obtained through chemical recycling of PLA onto PET substrates  
104 under atmospheric pressure conditions. The work focuses on (i) characterizing the chemical  
105 composition and morphology of the deposited layers, (ii) evaluating their hydrophilic  
106 properties, and (iii) assessing their antibacterial performance. By linking PLA waste chemical  
107 recycling with plasma deposition, this work establishes a link between chemical recycling of  
108 biopolymers and plasma surface engineering by demonstrating that methyl and ethyl lactate  
109 obtained from PLA can serve as effective precursors for the preparation of hydrophilic and  
110 antibacterial coatings on PET substrates.

## 111 2. Materials and methods

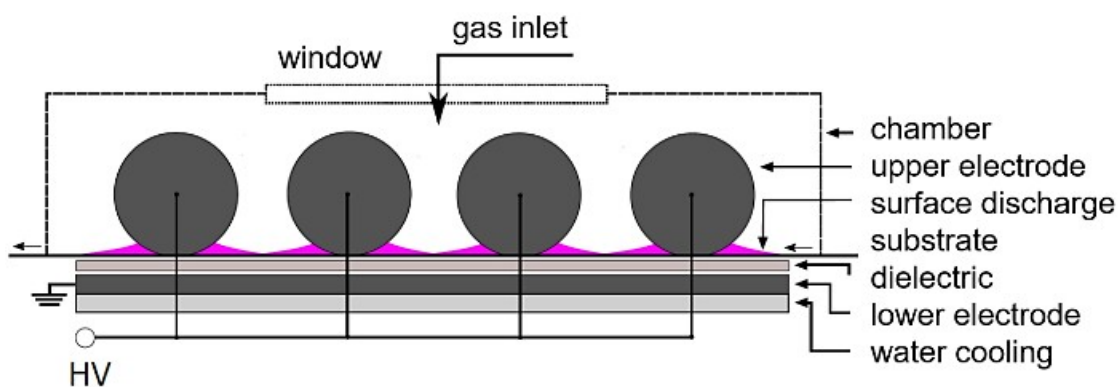
### 112 2.1 Materials

113 Polyethylene terephthalate (PET) films (TFP universal a.s., Dobřejovice, Czech Republic)  
114 with dimensions of 120 mm × 1000 mm and a thickness of 1 mm were used as substrates for  
115 deposition and served as a reference material. The monomers utilized for plasma deposition  
116 were ethyl lactate and methyl lactate, derived from virgin PLA (Ingeo™ 2003D,  
117 NatureWorks®, Minneapolis, USA), specifically prepared through the solvolysis process and  
118 their purity was determined as described by Domincova Bergerova et al. [12]. The bacterial  
119 strains *Staphylococcus aureus* (CCM 4516) and *Escherichia coli* (CCM 4517) were sourced  
120 from the Czech Collection of Microorganisms, Masaryk University (Brno, Czech Republic).

### 121 2.2 Sample preparation - plasma deposition

122 Plasma deposition was conducted according to Šťáhel et al. [13], with a few minor  
123 adjustments. PET films were prepared and served as the initial substrates for plasma  
124 deposition. Thin film plasma polymerization was performed in a specially designed reactor

125 equipped with a surface dielectric barrier discharge (SDBD) system. The reactor comprised  
126 three primary components: an electrode system, a cooling system, and a high-voltage  
127 generator. The complete deposition apparatus was situated within a fume hood throughout the  
128 deposition procedure, and the resultant gaseous products were continuously evacuated. The  
129 SDBD electrode setup consisted of 11 upper rotating cylindrical brass electrodes with a  
130 diameter of 1 cm and a length of 10.4 cm, spaced 2 mm apart. Below the cylindrical  
131 electrodes, a flat lower electrode of the size of 13.6 x 10 cm was positioned and covered with  
132 a 1 mm thick mica dielectric. The substrate was periodically moved along the upper and lower  
133 electrodes at a speed of 3 cm/min. As the upper electrodes rotated, they contacted the moving  
134 substrate. The lower electrode was grounded, whereas the upper electrodes were connected to  
135 a high-voltage AC power supply (Lifetech, Brno, Czech Republic) using a sinusoidal voltage  
136 with an amplitude of 11 kV and a frequency of 12 kHz. The power input to the system was set  
137 to 150 W. A schematic of the experimental setup is presented in Fig. 1.



138  
139 Figure 1: Schematic of the deposition setup [13]

140 As the working gas, nitrogen was used; it was supplied between the upper electrodes at a flow  
141 rate of 3 slm. The monomers ethyl lactate and methyl lactate as precursors were introduced  
142 into the nitrogen flow at rates ranging from 250 to 1000 sccm. The substrate passed through  
143 the discharge three times, with a total deposition time of 6.5 seconds. Throughout the  
144 deposition process, the apparatus was water-cooled to maintain a consistent electrode  
145 temperature.

## 146 2.3 Characterization of chemical structure

### 147 2.3.1 Fourier transform infrared spectroscopy with attenuated total reflection

148 Fourier transform infrared spectroscopy with attenuated total reflection (ATR-FTIR) spectra  
149 were recorded for all polymer films using a Nicolet iS5 spectrometer (Thermo Fisher

150 Scientific, Waltham, USA), equipped with a Ge crystal. The analysis was conducted over a  
151 range of 600–4000 cm<sup>-1</sup> with a resolution of 4 cm<sup>-1</sup>, and 64 scans were averaged per spectrum.  
152 Data processing was performed using OMNIC software (Thermo Fisher Scientific, Waltham,  
153 USA).

### 154 2.3.2 X-ray photoelectron spectroscopy

155 X-ray photoelectron spectroscopy (XPS) analysis was conducted using an ESCALAB 250Xi  
156 system (Thermo Fisher Scientific, East Grinstead, UK), utilizing an X-ray beam with a power  
157 output of 200 W and a spot size of 650 microns. Survey spectra were collected with a pass  
158 energy of 50 eV and an energy step of 1 eV, while high-resolution scans were performed with  
159 a pass energy of 20 eV and an energy step of 0.1 eV. To mitigate surface charging effects, an  
160 electron flood gun was employed. All spectra were referenced to the C1s hydrocarbon  
161 component with a binding energy of 284.8 eV. Data calibration, processing, and fitting were  
162 performed with Avantage software (version 5.9925).

### 163 2.4 Characterization of hydrophilic properties

164 The wettability of the sample surface was evaluated by measuring the static contact angle  
165 (CA) using a SEE System instrument (Advex Instruments, Czech Republic), equipped with a  
166 UVC camera and a high-resolution glass objective lens. Three test liquids were employed:  
167 ultrapure water (resistivity 18.2 MΩ·cm, Milli-Q, Merck), diiodomethane (≥99%, Sigma  
168 Aldrich), and ethylene glycol (≥99%, Sigma Aldrich). Droplets of 3 μL were deposited on the  
169 surface using a micropipette, and images were acquired approximately 1 s after deposition.  
170 For each liquid and sample, five independent measurements were performed, and the average  
171 values are reported. The images were analyzed using the SEE System software to determine  
172 the contact angle. The total surface free energy (γ<sup>tot</sup>) and its dispersive (γ<sup>d</sup>) and polar (γ<sup>p</sup>)  
173 components were calculated according to the **Owens–Wendt–Rabel–Kaelble (OWRK)**  
174 **method** [14], using the following relationship (1):

$$175 \quad \gamma_L(1 + \cos \theta) = 2 \left( \sqrt{\gamma_S^d \gamma_L^d} + \sqrt{\gamma_S^p \gamma_L^p} \right) \quad (1)$$

176 where  $\gamma_L$  and  $\gamma_S$  are the liquid and solid surface tensions, with dispersive (d) and polar (p)  
177 contributions.

### 178 2.5 Characterization of morphology

#### 179 2.5.1 Scanning electron microscopy

180 Scanning electron microscopy (SEM) images of the sample surfaces and fracture areas were  
181 obtained using a Nova NanoSEM 450 (FEI, USA). Prior to imaging, the samples were coated  
182 with a gold–palladium alloy to improve electrical conductivity; the coating was deposited by  
183 sputtering, which lasted 60 s and resulted in the film thickness of approximately 10 nm, with a  
184 grain size in the range of 3–5 nm. The SEM measurements were conducted at a working  
185 distance (WD) of 4.7 mm and an accelerating voltage (HV) of 5 kV.

#### 186 2.5.2 Atomic force microscopy

187 The surface topography of treated and untreated PET films was characterized using an atomic  
188 force microscope (AFM) model Dimension-Icon. Measurements were conducted at a scan  
189 rate of 1 Hz with a resolution of  $256 \times 256$  pixels in tapping mode under ambient air  
190 conditions. For the measurements, a silicon-nitride probe ScanAsyst-Air (both Bruker,  
191 Billerica, MA, USA) with a resonant frequency of 70 kHz and a stiffness constant of 0.4  
192  $\text{N}\cdot\text{m}^{-1}$  was employed.

#### 193 2.6 Characterization of antibacterial properties

194 The antibacterial properties of the samples were evaluated following the ISO 22196:2011  
195 standard. Prior to testing, the samples were disinfected with 70% denatured ethanol. Bacterial  
196 suspensions of *E. coli* ( $3.1 \times 10^5$  CFU/mL) and *S. aureus* ( $4.0 \times 10^5$  CFU/mL) were prepared  
197 in 1/500 nutrient broth (HiMedia laboratories, Mumbai, India). A 100  $\mu\text{L}$  aliquot of bacterial  
198 suspension was applied to the surface of the samples ( $25 \times 25$  mm), which were then covered  
199 with polypropylene foil ( $20 \times 20$  mm). Afterwards, the samples were incubated at 35 °C and  
200 100% relative humidity for 24 hours. Following incubation, the polypropylene foil was  
201 removed, and the samples were washed with soya casein digest lecithin polysorbate broth,  
202 which was subsequently collected.

203 The antibacterial activity was evaluated using equation (2):

$$204 \quad R = U_t - A_t \quad (2)$$

205 where  $R$  is the antibacterial activity,  $U_t$  means the common logarithm of the viable bacteria  
206 count ( $\text{CFU cm}^{-2}$ ) recovered from the untreated (blank) sample, and  $A_t$  stands for the count for  
207 the treated specimen after 24 hours [15].

208 For subsequent analyses, the plasma-treated samples at a flow rate of 1000 sccm were used.

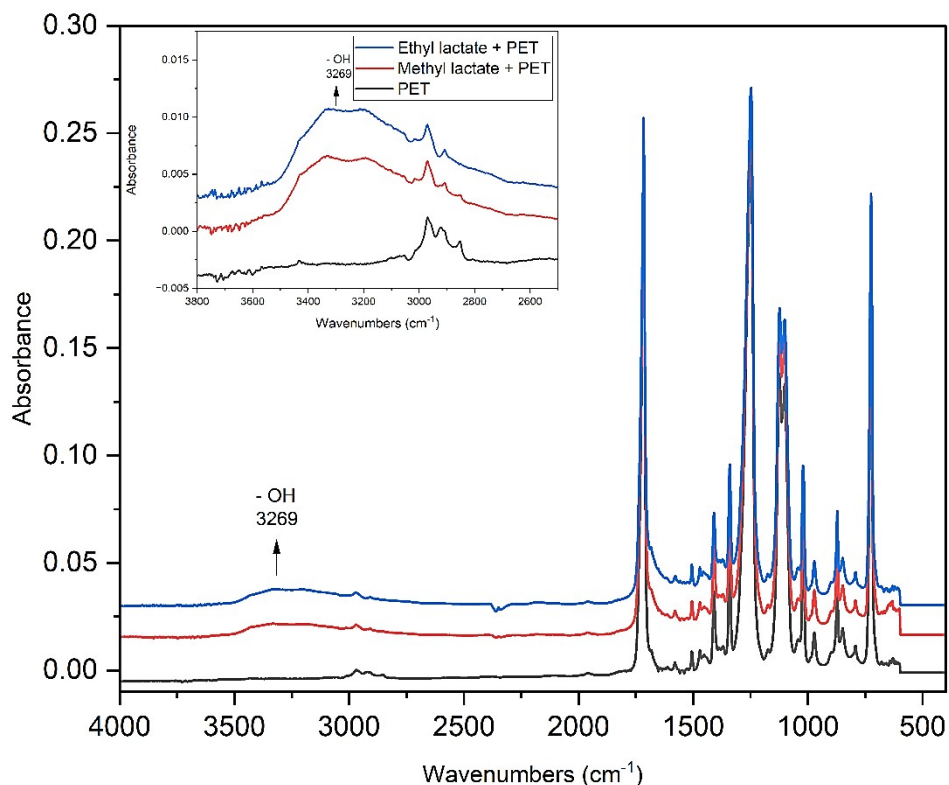
209

## 210 3 Results and discussion

### 211 3.1 Characterization of chemical structure

#### 212 3.1.1 ATR-FTIR Analysis

213 As seen in Figure 2, the ATR-FTIR spectra of all samples, including methyl lactate/PET,  
214 ethyl lactate/PET, and bare PET, exhibit near-identical profiles. Comparison of the spectra  
215 using the OMNIC software library revealed a greater than 99% match for all samples.  
216 Notably, the ethyl lactate/PET and the methyl lactate/PET samples exhibited changes in the  
217 region between 3500 and 2600  $\text{cm}^{-1}$ , corresponding to O-H or N-H bonds, which may  
218 contribute to increased hydrophilicity [16]. The spectral similarity suggests that the deposited  
219 plasma films are relatively thin, with the FTIR signal predominantly influenced by the  
220 underlying PET substrate. Moreover, as no previous studies have reported FTIR spectra for  
221 plasma-treated ethyl lactate and methyl lactate, this aspect remains insufficiently understood  
222 and warrants further systematic investigation.



223

224 Figure 2: FTIR spectra of samples: methyl lactate/PET (flow rate 1000 sccm), ethyl  
225 lactate/PET (flow rate 1000 sccm) and bare PET.

226 3.1.2 Surface composition of samples

227 The surface composition of samples was followed with X-ray photoelectron spectroscopy and  
 228 the results are summarized in Table 1. As can be seen, the reference PET sample exhibits 74%  
 229 carbon and 24% oxygen, which is consistent with theoretical expectations [17]. The O/C ratio,  
 230 indicative of increased surface oxygen-containing functionalities, is 0.324. For the plasma-  
 231 modified methyl lactate/PET sample, the surface consists of 61% carbon, 27% oxygen, and  
 232 11% nitrogen, resulting in an increased O/C ratio of 0.443. In the case of the ethyl lactate/PET  
 233 sample, nitrogen content was markedly higher reaching 25%, with oxygen also present at  
 234 25%, and carbon at 50%. The O/C ratio for this sample is 0.5, representing an over 1.5-fold  
 235 increase compared to the reference PET sample. These results indicate substantial surface  
 236 functionalization following plasma deposition.

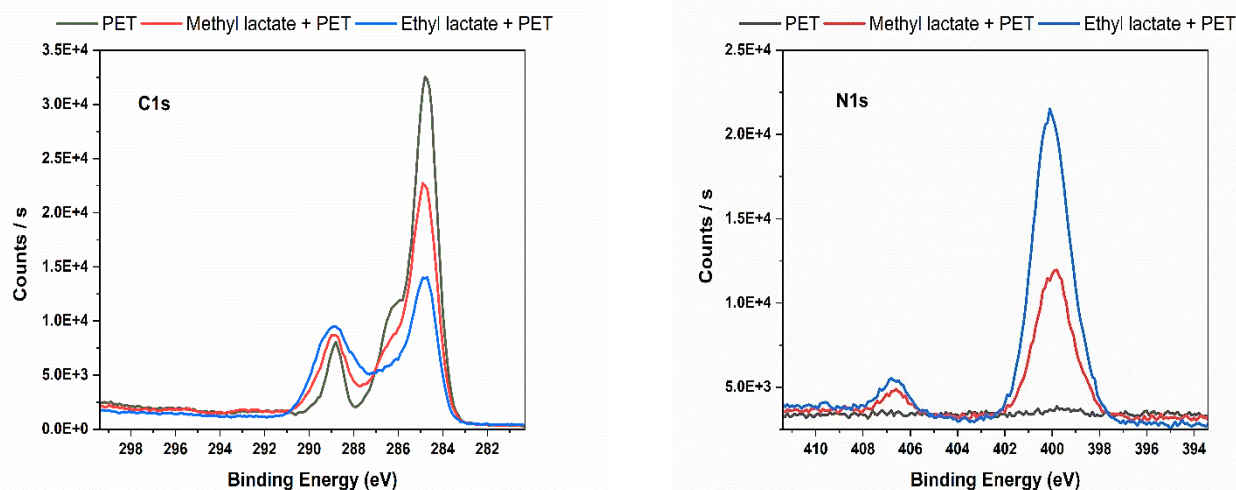
237

238 Table 1 Sample elemental surface composition (%) and bond distributions (%) according to  
 239 XPS analysis. Samples: methyl lactate/PET (flow rate 1000 sccm), ethyl lactate/PET (flow  
 240 rate 1000 sccm) and bare PET.

		<b>PET reference</b>	<b>methyl lactate/PET</b>	<b>ethyl lactate/PET</b>
		<b>(%)</b>	<b>(%)</b>	<b>(%)</b>
	<b>C</b>	74	61	50
	<b>O</b>	24	27	25
	<b>N</b>	0	11	25
<b>C1s</b>	<b>C=C</b>	15	11	6
	<b>C-C/C-H</b>	50	45	28
	<b>C-N</b>	0	8	13
	<b>C-O</b>	23	13	10
	<b>C=O</b>	0	2	8
	<b>N-C=O</b>	0	3	10
	<b>COO</b>	12	18	25
<b>N1s</b>	<b>-C=N</b>	-	5	5
	<b>-C-NH-</b>	-	69	57
	<b>-CONH-</b>	-	16	30
	<b>nitrate</b>	-	10	8

241

242 For a more detailed analysis of the effect of plasma modification, high-resolution XPS spectra  
243 of the C1s and N1s were measured (Figure 3). The figure reveals distinct differences in  
244 surface chemistry between the reference PET and the plasma-modified samples, with  
245 variations also observed between the methyl and ethyl lactate treatments. Deconvolution of  
246 these spectra provided further insights into the formation of different functional groups.



248 Figure 3: Overlay of XPS C1s and N1s spectra of the PET reference and plasma modified  
249 samples (methyl lactate/PET and ethyl lactate/PET).

250

251 The C1s spectra of the reference PET sample were deconvoluted into four distinct peaks with  
252 binding energies of 284.5 eV, 284.8 eV, 286.4 eV, and 289 eV, corresponding to carbon  
253 atoms in C=C, C-C/C-H, C-O, and COO functional groups, respectively. Following plasma  
254 modification, three additional peaks emerged at binding energies of 285.7 eV, 287.7 eV, and  
255 288.4 eV, which are assigned to C-N, C=O, and N-C=O functional groups, respectively  
256 (Figure 4) [18],[19], [20],[21],[22] . The relative concentrations of all detected carbon  
257 functional groups on the surface of the analyzed samples are presented above in Table 1.

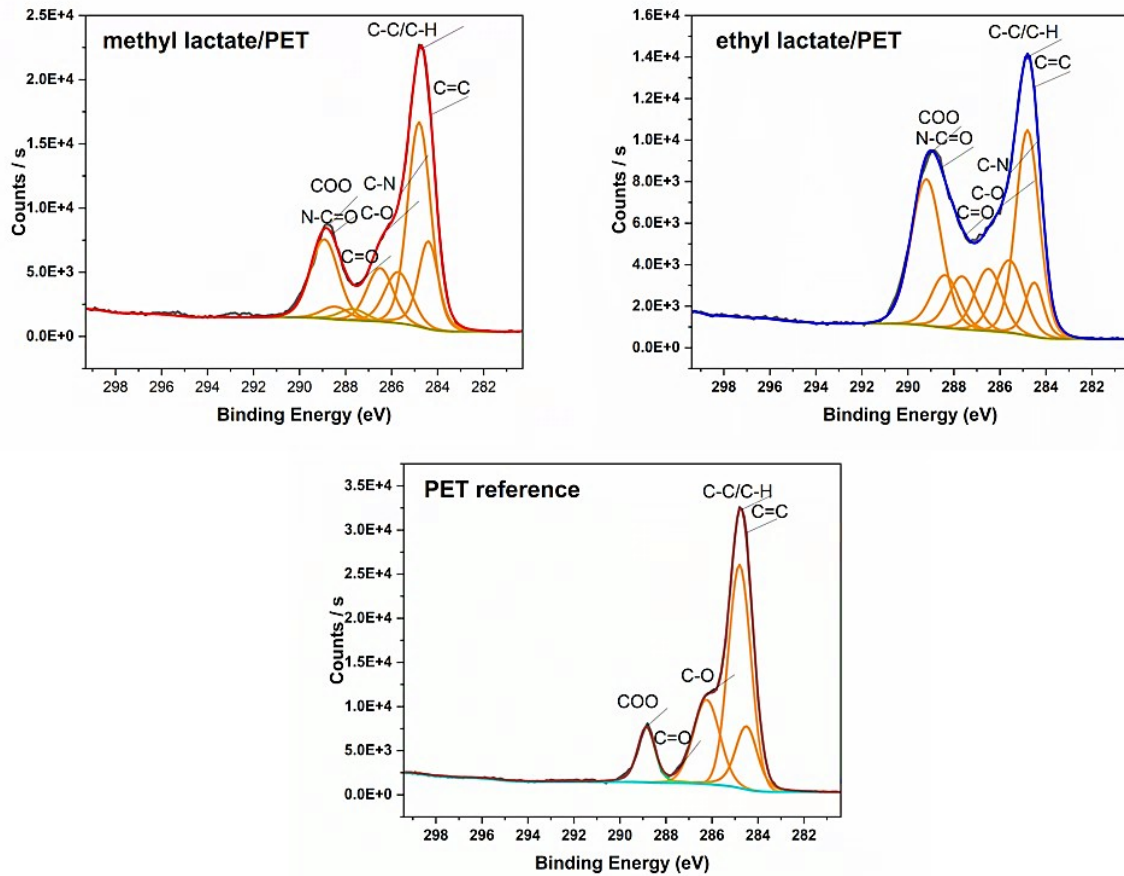
258 Deconvolution of the C1s spectra reveals a progressive reduction in the relative contributions  
259 of nonpolar carbon environments (C=C and C-C/C-H) compared to the reference PET. The  
260 fraction of C=C bonds decreases from 15% in pristine PET to 11% in methyl lactate/PET and  
261 to 6% in ethyl lactate/PET, while C-C/C-H bonds drop from 50% to 45% and 28%,

262 respectively. Importantly, this decrease does not indicate chemical consumption or  
263 transformation of the aromatic structures of PET. Rather, it reflects attenuation of the XPS  
264 signal from the underlying polymer due to coverage by a thin plasma-deposited film. Because  
265 XPS probes only the outermost nanometers of the surface, the detected bonding environment  
266 primarily represents the newly formed coating rather than the bulk PET substrate.  
267 Concurrently, there is a pronounced increase in polar oxygen- and nitrogen-containing  
268 functional groups. Signals assigned to C–N, C=O, N–C=O, and COO groups emerge or  
269 increase significantly after plasma deposition. The COO contribution rises from 12% in the  
270 reference PET to 18% in methyl lactate/PET and 25% in ethyl lactate/PET, while C–N and  
271 N–C=O functionalities are absent in pristine PET but clearly present in both modified  
272 samples. These changes confirm that plasma-assisted deposition introduces a highly  
273 functionalized surface layer enriched in ester, carbonyl, amide, and amine-related structures,  
274 which are expected to increase surface polarity and hydrophilicity.

275 The N1s spectra further support this interpretation. The plasma-treated samples display peaks  
276 corresponding to imine (–C=N, 398.6 eV), amine (–C–NH–, 400 eV), amide (–CONH–, 401.0  
277 eV), and nitrate ( $\text{NO}_3^-$ , 406.7 eV) functionalities (Figure 5). Nitrogen is incorporated  
278 predominantly in the form of amine groups, which represent the major nitrogen species in  
279 both ester-derived coatings. In addition, amide and imine functionalities are detected, together  
280 with minor contributions attributed to nitrate species. The ethyl lactate/PET sample shows a  
281 higher fraction of amide groups and an overall nitrogen content approximately twice that of  
282 the methyl lactate/PET sample, indicating more extensive nitrogen-containing  
283 functionalization.

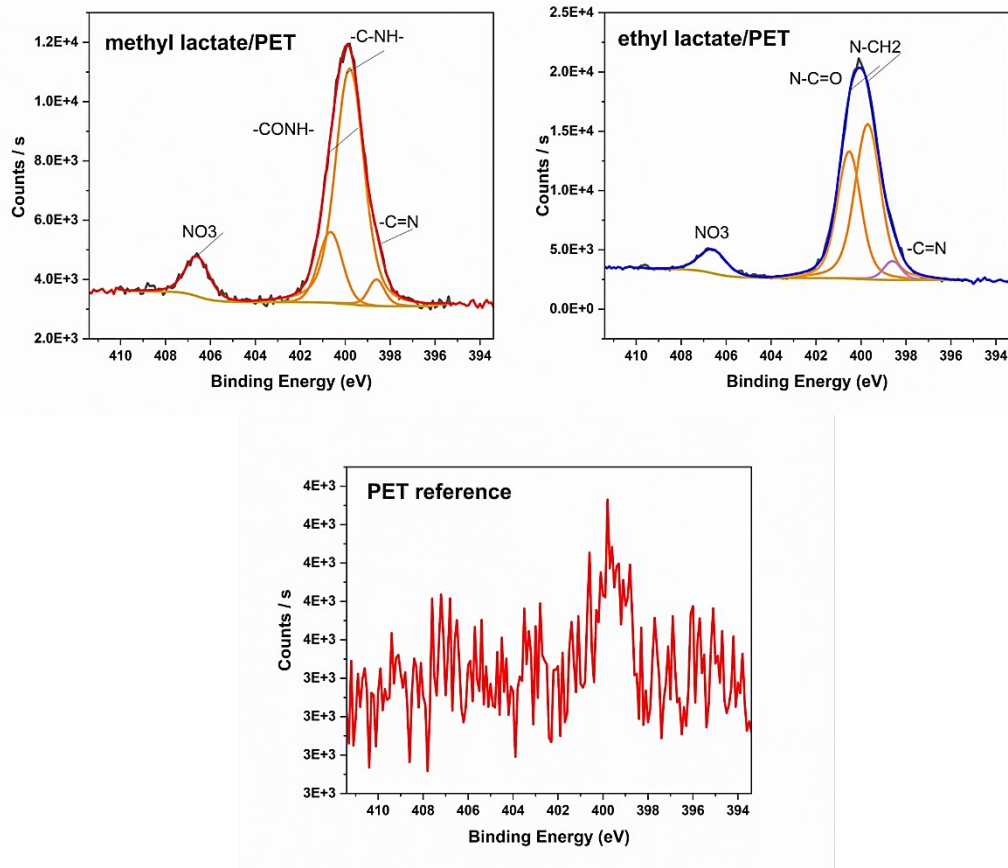
284 Overall, the XPS results confirm successful plasma-assisted deposition of ester-derived  
285 coatings onto PET. The observed spectral changes are governed by the formation of a new,  
286 thin, heteroatom-rich surface layer that masks the underlying PET signal, rather than by  
287 chemical modification of the PET backbone itself. Among the two precursors, ethyl lactate  
288 leads to a more strongly functionalized surface, characterized by higher nitrogen  
289 incorporation and a greater abundance of carbonyl- and amide-related groups. These surface  
290 chemical changes are consistent with the observed enhancement in hydrophilicity and are  
291 likely to contribute to the functional performance of the coatings.

292



293

294 Figure 4: High-resolution XPS C1s spectra of the PET reference and plasma-modified  
 295 methyl lactate/PET and ethyl lactate/PET samples.



296

297 Figure 5: High-resolution XPS N1s spectra of the PET reference and plasma-modified  
 298 methyl lactate/PET and ethyl lactate/PET samples.

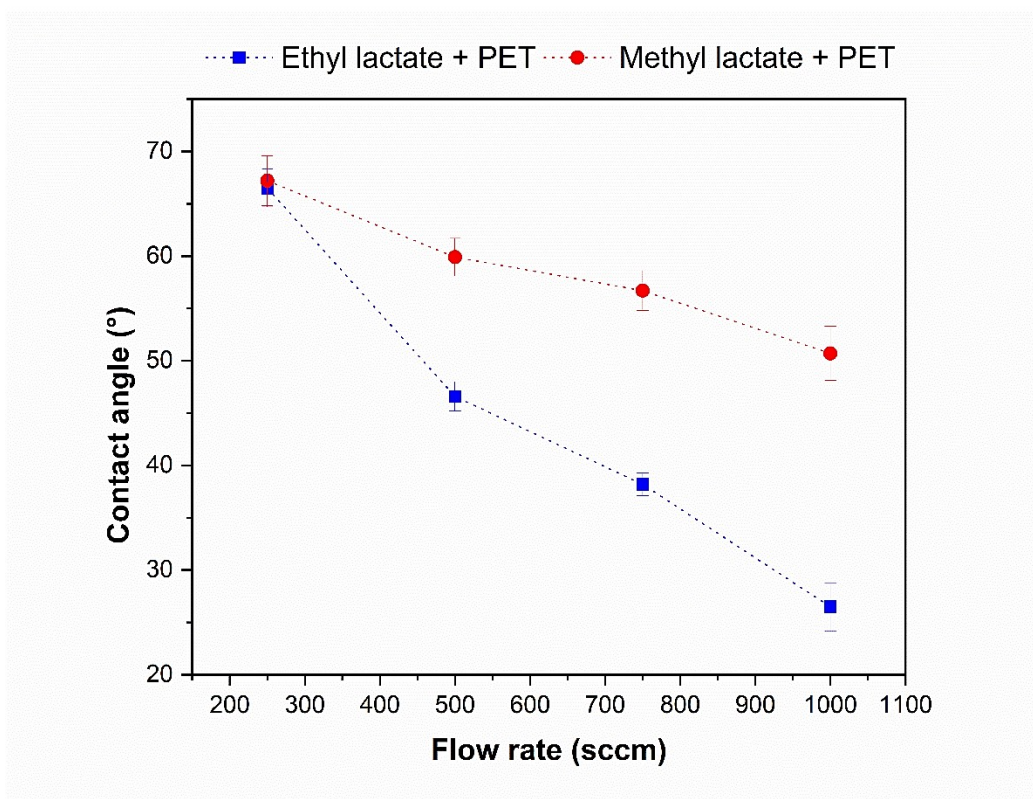
299

### 300 3.2 Hydrophilicity of materials - contact angle and surface energy evaluation

301 The contact angle (CA) values and calculated surface free energy (SFE) of the samples are  
 302 summarized in Table 2. Water CA values serve as a qualitative indicator of hydrophilic versus  
 303 hydrophobic character, whereas the complete set of contact angles obtained with different  
 304 probe liquids is required for quantitative SFE analysis.

305 As shown in Table 2, plasma modification progressively enhanced the hydrophilic properties  
 306 of both ethyl lactate and methyl lactate coatings. For ethyl lactate, the most pronounced  
 307 hydrophilicity was observed at a monomer flow rate of 1000 sccm, with a water CA of  $27 \pm$   
 308  $2^\circ$ . In contrast, the lowest CA achieved for methyl lactate under the same conditions was  $51 \pm$   
 309  $3^\circ$ . These results indicate that ethyl lactate plasma layers introduce a higher density of polar  
 310 functionalities than methyl lactate, consistent with XPS findings that revealed greater  
 311 incorporation of oxygen- and nitrogen-containing groups. Such a pronounced difference in  
 312 wettability is particularly relevant, as previous studies have shown that only surfaces with

313 very low water contact angles (below  $\sim 30^\circ$ ) are capable of sustaining stable hydration layers  
314 that effectively alter interfacial interactions [23,24]. The evolution of water CA values for  
315 both coatings is presented graphically in Figure 6.



316

317 Figure 6: The water contact angle values for plasma-polymerized ethyl lactate/PET and  
318 methyl lactate/PET films (RSD =  $3 \pm 1$ ).

319 The Owens–Wendt analysis further confirmed that plasma treatment predominantly increased  
320 the polar contribution ( $\gamma^p$ ) of SFE, while the dispersive part ( $\gamma^d$ ) remained nearly  
321 unchanged. For example, ethyl lactate at 1000 sccm exhibited a total SFE of  $60 \text{ mJ}\cdot\text{m}^{-2}$  with a  
322 dominant polar fraction, compared to only  $46 \text{ mJ}\cdot\text{m}^{-2}$  for untreated PET. This trend is  
323 supported by XPS (Table 1), which detected incorporation of polar oxygen- and nitrogen-  
324 containing groups ( $-\text{OH}$ ,  $-\text{C}=\text{O}$ ,  $-\text{C}-\text{N}$ ,  $\text{N}-\text{C}=\text{O}$ ). Importantly, FTIR spectroscopy (Figure 2)  
325 provided complementary evidence, revealing a more pronounced presence of  $-\text{OH}$   
326 functionalities in ethyl lactate compared to methyl lactate coatings. In sum, the XPS and FTIR  
327 results converge on the conclusion that plasma deposition promotes the incorporation of  
328 hydroxyl and nitrogen-containing groups, which are directly responsible for the enhanced  
329 surface polarity and hydrophilicity.

330 Comparable trends have been documented for other plasma-modified polymers. Lai et al.  
 331 demonstrated that plasma treatment of polymers results in a significant decrease in water CA  
 332 and a corresponding increase in SFE, primarily due to oxygen incorporation [25]. Johnston  
 333 and Ratner reported that plasma-polymerized organic films exhibit a marked increase in  $\gamma^p$   
 334 following the introduction of heteroatom-containing moieties [26], while Cui and Brown  
 335 showed that in plasma-treated polypropylene the rise in SFE is attributable predominantly to  
 336  $\gamma^p$  [27]. More recent work corroborates these findings, including the deposition of  
 337 nanocomposite coatings from ethyl lactate [27] and rapid hydrophilization via atmospheric  
 338 plasma polymerization [28].

339 Analogous effects of plasma treatment on the enhancement of surface polarity and wettability  
 340 have also been reported for polycarbonate [29], PET films modified by plasma-based ion  
 341 implantation [30], and PET track membranes [31], underlining the universal nature of plasma-  
 342 induced hydrophilization across diverse polymeric systems.

343 Overall, both the present data and the literature consistently indicate that the hydrophilization  
 344 of PET surfaces coated with plasma-polymerized lactate esters originates from the  
 345 introduction of polar functional groups, particularly hydroxyl and nitrogen species, leading to  
 346 an increase in  $\gamma^p$  that clearly outweighs changes in dispersive interactions.

347 Table 2 Contact angles of plasma-polymerized films deposited at different monomer flow  
 348 rates. The PET reference represents the untreated substrate.

Sample	Flow Rate (sccm)	Contact Angle (°)			Surface Free Energy (mJ/m <sup>2</sup> )
		Water	CH <sub>2</sub> I <sub>2</sub>	Ethylene glycol	Total
0. PET reference	/	76 ± 1	27 ± 1	31 ± 1	46
1. ethyl lactate/PET	250	67 ± 2	32 ± 1	36 ± 1	48
2. ethyl lactate/PET	500	47 ± 1	33 ± 2	29 ± 1	55
3. ethyl lactate/PET	750	38 ± 1	33 ± 2	25 ± 0	55
4. ethyl lactate/PET	1000	27 ± 2	46 ± 2	29 ± 2	60

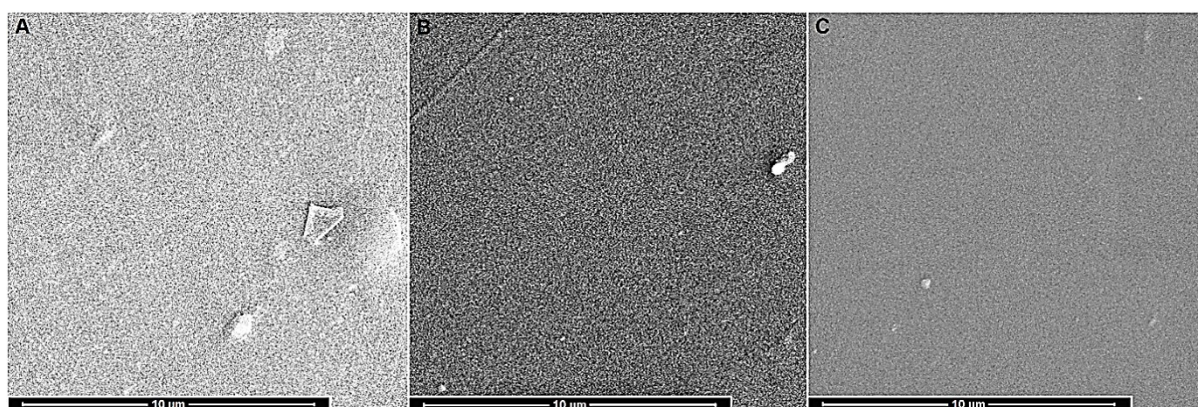
5. methyl lactate/PET	250	$67 \pm 2$	$30 \pm 3$	$27 \pm 3$	50
6. methyl lactate/PET	500	$60 \pm 2$	$32 \pm 1$	$36 \pm 2$	50
7. methyl lactate/PET	750	$57 \pm 2$	$37 \pm 2$	$23 \pm 2$	51
8. methyl lactate/PET	1000	$51 \pm 3$	$48 \pm 2$	$48 \pm 1$	50

### 349 3.3 Morphology of the tested materials

#### 350 3.3.1 Scanning electron microscopy

351 Figure 7 illustrates the surface morphology of PET in response to plasma treatment. Figure  
 352 7A presents a typical image of untreated PET film, characterized predominantly by the  
 353 presence of irregular protrusions on the surface. In contrast, plasma-treated samples, depicted  
 354 in Figures 7B and 7C, exhibit notable modifications in surface topography. Although some  
 355 irregular protrusions remain visible following plasma treatment, the overall surface appears  
 356 considerably smoother. Moreover, Figure 7C demonstrates an even greater degree of surface  
 357 smoothness compared to the untreated PET, with only a few residual protrusions observed.

358 These findings suggest that a substantial number of micrometer-scale protrusions are  
 359 effectively reduced or eliminated, a phenomenon that can be primarily attributed to the  
 360 bombardment of the sample surface by energetic particles generated during the plasma  
 361 treatment process [25].



362  
 363 Figure 7: Representative SEM images of PET sample surfaces, obtained at approximately  
 364  $10,000\times$  magnification (scale bar:  $10\ \mu\text{m}$ ), illustrating surface morphology variations: (A)  
 365 untreated PET film, (B) ethyl lactate plasma-treated sample (nitrogen flow rate: 1000 sccm),  
 366 and (C) methyl lactate plasma-treated sample (nitrogen flow rate: 1000 sccm).

### 367 3.3.2 Atomic force microscopy

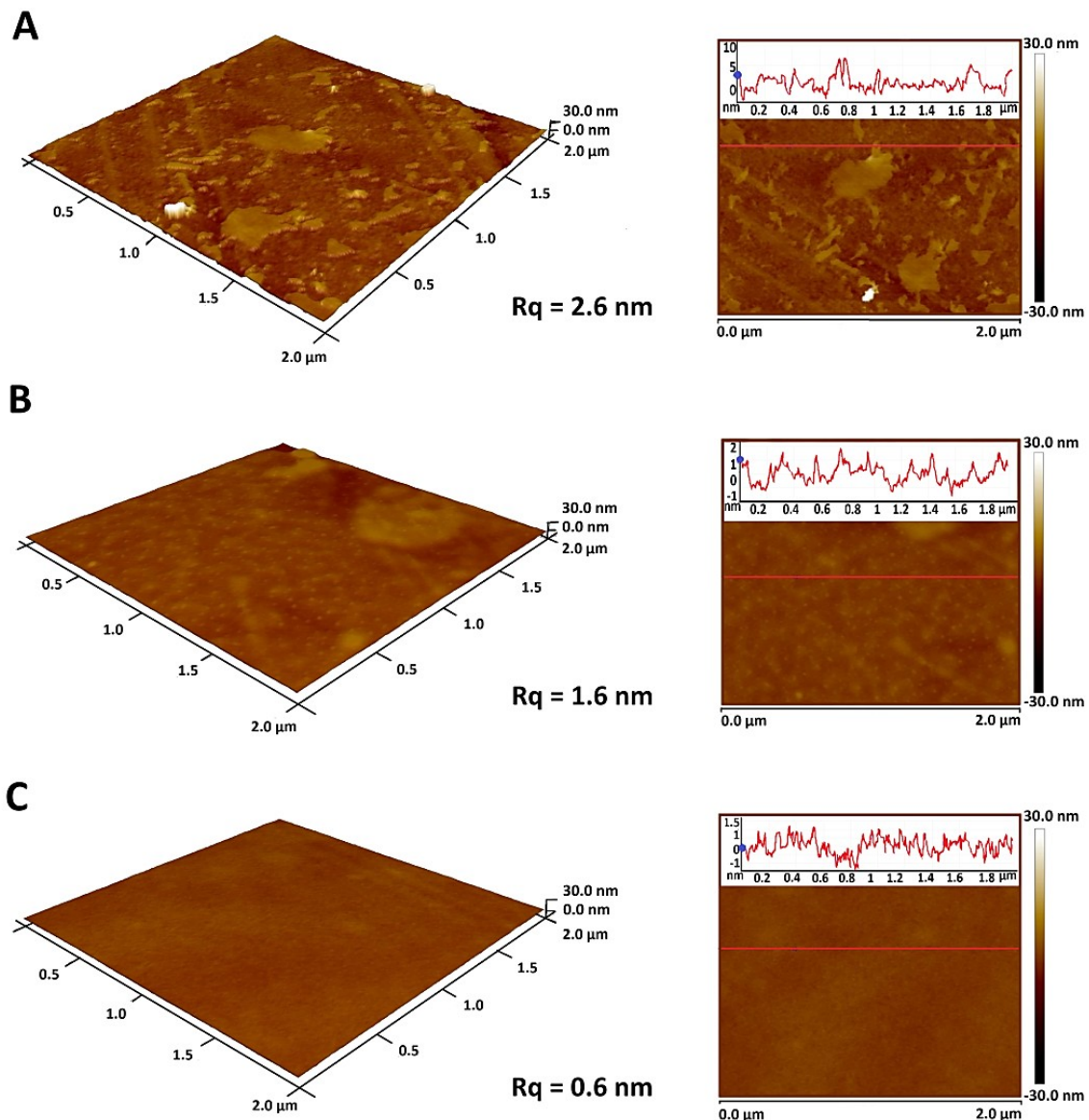
368 Figure 8 presents atomic force microscopy (AFM) images illustrating the surface topography  
369 of samples. The surface topography of a reference sample, untreated polyethylene  
370 terephthalate (PET) film, was analyzed using AFM in tapping mode. Similarly, the surface  
371 morphology of samples coated with plasma-prepared layers of methyl lactate/PET and ethyl  
372 lactate/PET was examined under identical conditions. The scanned surface area measured  $2 \times$   
373  $2 \mu\text{m}$ . The images on the left part of the figure depict three-dimensional representations of the  
374 individual samples, while the corresponding two-dimensional models are displayed on the  
375 right.

376 The untreated PET surface exhibits a heterogeneous morphology with relatively pronounced  
377 nanoscale undulations and irregular height fluctuations reaching approximately 60 nm. This  
378 morphology is typical for semi-crystalline PET films and reflects the coexistence of  
379 amorphous and crystalline domains formed during film processing. The root mean square  
380 roughness of pristine PET ( $R_q \approx 2.6 \text{ nm}$ ) indicates a comparatively heterogeneous surface  
381 with locally exposed microstructural features [32].

382 Following plasma deposition, both modified samples show a substantial transformation of the  
383 original PET topography, confirming the formation of a continuous plasma-polymerized  
384 layer. The ethyl lactate/PET surface is characterized by a fine granular nanostructure  
385 composed of uniformly distributed nanoscale features, with height variations on the order of  
386 several nanometers and a reduced roughness ( $R_q \approx 1.6 \text{ nm}$ ). This observation aligns with the  
387 findings of Milaniak et al., who reported that plasma polymerization of ethyl lactate results in  
388 a less pronounced surface roughness [33]. In contrast, the methyl lactate/PET sample displays  
389 a more homogeneous and smoother morphology with smaller, more compact nanoscale  
390 features, also exhibiting height variations on the order of several nanometers and a further  
391 reduction in roughness ( $R_q \approx 0.6 \text{ nm}$ ). The smoother morphology suggests the formation of a  
392 denser and more uniform plasma polymer layer, which may be attributed to differences in  
393 precursor fragmentation pathways and polymerization kinetics. Similar morphology evolution  
394 has been reported for plasma polymer films derived from oxygen-containing organic  
395 precursors, where film densification and uniform growth lead to reduced nanoscale roughness  
396 [34,35]

397 In conclusion, from a functional perspective, the nanoscale roughness values of all plasma-  
398 modified samples remain in the low-roughness regime. The combination of reduced

399 roughness and increased surface polarity promotes the formation of stable hydration layers,  
400 which are known to influence wettability and bacterial adhesion [36].



401

402 Figure 8: Atomic force microscopy representations of the surface topography of samples: A)  
403 untreated PET film, B) ethyl lactate plasma-treated sample (flow rate 1000 sccm), C) methyl  
404 lactate plasma-treated sample (flow rate 1000 sccm).

405

### 406 3.4 Antibacterial properties of the tested materials

407 The antibacterial activity of the prepared films was evaluated in accordance with the  
408 international standard ISO 22196:2011 [15]. The assessment was conducted on sample films  
409 containing methyl lactate and ethyl lactate, using *E. coli* as a representative gram-negative

410 bacterial strain and *S. aureus* as an example of gram-positive strain. As can be seen in Table  
411 3, samples with methyl lactate exhibit greater antimicrobial efficacy. Notably, sample 6,  
412 deposited at a flow rate of 500 sccm, demonstrated strong antibacterial activity (R=3.4)  
413 against *E. coli* and significant activity (R=2.1) against *S. aureus*. Furthermore, sample 5 has  
414 been found to be particularly relevant, as it exhibits significant antimicrobial properties  
415 against both tested bacterial strains.

416 This antibacterial activity may be associated with the presence of amines, as suggested by  
417 XPS analysis. Several studies have confirmed that amines possess notable antibacterial  
418 properties [37–39]. Mentheour et al. reported that the antibacterial effects were primarily  
419 linked to enhanced hydrophilicity resulting from amines generated by reactive nitrogen  
420 species (RNS) within the dielectric barrier discharge (DBD) plasma source [40].

421 In general, surfaces exhibiting moderate wettability tend to facilitate bacterial or cellular  
422 adhesion more effectively than surfaces that are either highly hydrophobic or extremely  
423 hydrophilic. Additionally, an increase in surface free energy (Table 2), particularly in its polar  
424 or acid-base components, along with an enhancement of the electron donor character of the  
425 substrate, has been shown to reduce bacterial adhesion [36,41]. The bacterial-repellent  
426 properties of hydrophilic surfaces can be attributed to the formation of a hydration layer on  
427 PET-treated surfaces. This hydration layer, arising from the hydrophilic and polar nature of  
428 the surface, generates hydration forces that inhibit the attachment of non-specific proteins and  
429 microorganisms [42].

430 Surface roughness is another critical factor that can inhibit bacterial adhesion by increasing  
431 the available surface area for cell attachment and reducing the shear force of the flowing fluid.  
432 This reduction in shear force helps prevent the detachment of adhered bacteria [41].  
433 However, nanoscale surface roughness has been found to exhibit the most effective anti-  
434 adhesion properties, whereas microscale roughness tends to promote bacterial adhesion. In  
435 contrast, smooth surfaces influence bacterial behaviour primarily through other material  
436 properties, such as surface chemistry and surface energy [36].

437 It should be noted that the long-term stability of the antibacterial properties was not evaluated  
438 in the present study and will be the subject of future investigation.

439 Table 3 Antibacterial activity (R) of films containing methyl lactate and ethyl lactate,  
440 deposited at varying monomer flow rates, against gram-positive and gram-negative bacterial  
441 strains after 24 hours of incubation.

Samples	<i>Staphylococcus aureus</i>		<i>Escherichia coli</i>	
	CCM 4516		CCM 4517	
	$N_x(\text{cfu}/\text{cm}^2)$	R	$N_x(\text{cfu}/\text{cm}^2)$	R
0. PET reference	$2.4 \times 10^5$	$U_t = 5.4$	$1.6 \times 10^6$	$U_t = 6.2$
1. ethyl lactate/PET	$1.0 \times 10^5$	0.4	$4.3 \times 10^5$	0.6
2. ethyl lactate/PET	$2.6 \times 10^4$	1.0	$2.9 \times 10^5$	0.7
3. ethyl lactate/PET	$6.8 \times 10^4$	0.5	$1.5 \times 10^5$	1.1
4. ethyl lactate/PET	$3.1 \times 10^4$	0.9	$3.9 \times 10^5$	0.6
5. methyl lactate/PET	$1.2 \times 10^3$	2.3	$1.7 \times 10^4$	2.0
6. methyl lactate/PET	$1.9 \times 10^3$	2.1	$6.5 \times 10^2$	3.4
7. methyl lactate/PET	$6.1 \times 10^4$	0.6	$4.2 \times 10^5$	0.6
8. methyl lactate/PET	$9.2 \times 10^4$	0.4	$2.8 \times 10^5$	0.8

442

#### 443 **4 Conclusion**

444 In this study, lactate esters were obtained through the environmentally sustainable chemical  
 445 recycling of a biopolymer and subsequently modified via plasma deposition. This process  
 446 enabled the development of a method for depositing antibacterial films on PET surfaces.

447 ATR-FTIR spectroscopy confirmed the presence of O–H bonds associated with the enhanced  
 448 hydrophilicity of the samples, particularly in the ethyl lactate-based coating (sample 3).  
 449 Complementary insights were provided by XPS analysis, which revealed the formation of  
 450 oxygen- and nitrogen-containing functional groups, with C=O, C–N, and N–C=O bonds being  
 451 most pronounced in the ethyl lactate/PET sample. Considering that XPS probes only the top  
 452 ~5–10 nm of the surface, whereas ATR-FTIR provides information from depths up to the  
 453 micrometer scale, the combined use of these techniques enables a comprehensive evaluation  
 454 of both surface-specific and bulk-like chemical characteristics. Although the film thickness  
 455 was not measured directly, it is reasonable to assume that it falls within the range of tens to  
 456 hundreds of nanometers, as reported based on comparable atmospheric-pressure plasma  
 457 polymerization systems.

458 The chemical composition and surface morphology analyses revealed significant differences  
 459 in topography between plasma-treated and untreated samples. Notably, the plasma-treated  
 460 films exhibited antibacterial properties against both *S. aureus* and *E. coli* in comparison to

461 untreated PET film. This antibacterial effect may be attributed to the hydrophilicity of the  
462 coatings and the presence of amines.

463 The plasma deposition of degradation products derived from the chemical recycling of  
464 biopolymers presents a novel approach to sustainable material development within the  
465 framework of the circular economy. This method not only introduces materials with enhanced  
466 functional properties but also offers an innovative strategy for sustainable waste management  
467 by utilizing chemically recycled polylactic acid esters.

468

#### 469 **CRedit authorship contribution statement**

470 Monika Strašáková: Writing – original draft, Visualization, Validation, Methodology,  
471 Investigation, Data curation, Conceptualization. Eva Domincová Bergerová: Project  
472 administration, Methodology, Investigation, Conceptualization, Marián Lehocký:  
473 Methodology, Investigation. Veronika Hanuliak: Methodology, Investigation. Hana  
474 Pištěková: Methodology, Investigation. Michal Urbánek: Methodology, Investigation. Pavel  
475 Šťáhel: Methodology, Investigation. Monika Stupavská: Methodology, Investigation. Jakub  
476 Klaban: Methodology, Investigation. Anežka Lengálová: Writing – review & editing.  
477 Vladimír Sedlařík: Supervision, Funding acquisition, Formal analysis.

478

#### 479 **Declaration of competing interest**

480 The authors declare that they have no conflict of interest.

481

#### 482 **Acknowledgements**

483 This work was supported from the European Just Transition Fund within the Operational  
484 Programme: Just Transition under the aegis of the Ministry of the Environment of the Czech  
485 Republic, project CirkArena number CZ.10.03.01/00/22\_003/0000045 and the Ministry of  
486 Education Youth and Sports of the Czech Republic, Operational Programme Johannes Amos  
487 Comenius OP JAC "Application potential development in the field of polymer materials in  
488 the context of circular economy compliance (POCEK)", number  
489 CZ.02.01.01/00/23\_021/0009004. Authors are further grateful for co-funding from the  
490 development process of Centre of Polymer Systems, Tomas Bata University in Zlin, program

491 DKRVO (RP/CPS/2024-28/002), (RP/CPS/2024-28/005), (RP/CPS/2024-28/007) and the  
492 Internal Grant Agency of the Centre of Polymer Systems in Zlin (IGA/CPS/2025/002)  
493 supported by the Ministry of Education Youth and Sports of the Czech Republic. One of the  
494 authors, M. Stupavská, gratefully acknowledges financial support from the Ministry of  
495 Education, Youth, and Sports of the Czech Republic under project LM2023039.

496

#### 497 **Data availability**

498 Data will be made available on request.

499

#### 500 **References**

501 World Economic Forum, Ellen MacArthur Foundation and McKinsey & Company, The New  
502 Plastics Economy: Rethinking the future of plastics, 2016.

503 R. Geyer, J.R. Jambeck, K.L. Law, Production, use, and fate of all plastics ever made, *Sci.*  
504 *Adv.* 3 (2017). [https://doi.org/10.1126/SCIADV.1700782/SUPPL\\_FILE/1700782\\_SM.PDF](https://doi.org/10.1126/SCIADV.1700782/SUPPL_FILE/1700782_SM.PDF).

505 P. Majgaonkar, R. Hanich, F. Malz, R. Brüll, Chemical Recycling of Post-Consumer PLA  
506 Waste for Sustainable Production of Ethyl Lactate, *Chemical Engineering Journal* 423 (2021)  
507 129952. <https://doi.org/10.1016/J.CEJ.2021.129952>.

508 I.S. Bayer, S. Guzman-Puyol, J.A. Heredia-Guerrero, L. Ceseracciu, F. Pignatelli, R. Ruffilli,  
509 R. Cingolani, A. Athanassiou, Direct transformation of edible vegetable waste into  
510 bioplastics, *Macromolecules* 47 (2014) 5135–5143. <https://doi.org/10.1021/MA5008557>.

511 M.N. Siddiqui, H.H. Redhwi, A.A. Al-Arfaj, D.S. Achilias, M.N.; Siddiqui, H.H.; Redhwi,  
512 A.A.; Al-Arfaj, D.S. Achilias, Chemical Recycling of PET in the Presence of the Bio-Based  
513 Polymers, PLA, PHB and PEF: A Review, (2021). <https://doi.org/10.3390/su131910528>.

514 A. Carné Sánchez, S.R. Collinson, The selective recycling of mixed plastic waste of  
515 polylactic acid and polyethylene terephthalate by control of process conditions, *Eur. Polym. J.*  
516 47 (2011) 1970–1976. <https://doi.org/10.1016/J.EURPOLYMJ.2011.07.013>.

517 H. Biederman, Plasma Polymer Films, *Plasma Polymer Films* (2004).  
518 <https://doi.org/10.1142/P336>.

- 519 R. Chakraborty, A. Govind Anoop, A. Thakur, G. Chandra Mohanta, P. Kumar, Strategies To  
520 Modify the Surface and Bulk Properties of 3D-Printed Solid Scaffolds for Tissue Engineering  
521 Applications, 8 (2023) 5139–5156. <https://doi.org/10.1021/acsomega.2c05984>.
- 522 N. Milaniak, G. Laroche, F. Massines, Atmospheric-pressure plasma-enhanced chemical  
523 vapor deposition of nanocomposite thin films from ethyl lactate and silica nanoparticles,  
524 Plasma Processes and Polymers 18 (2021) 2000153.  
525 <https://doi.org/10.1002/PPAP.202000153>.
- 526 B. Nisol, F. Reniers, Challenges in the characterization of plasma polymers using XPS, J.  
527 Electron Spectros. Relat. Phenomena 200 (2015) 311–331.  
528 <https://doi.org/10.1016/J.ELSPEC.2015.05.002>.
- 529 M. Laurent, E. Desjardins, M. Meichelboeck, N. Naudé, L. Stafford, N. Gherardi, G. Laroche,  
530 Characterization of argon dielectric barrier discharges applied to ethyl lactate plasma  
531 polymerization, J. Phys. D Appl. Phys. 50 (2017) 475205. <https://doi.org/10.1088/1361-5326463/AA916D>.
- 532 6463/AA916D.
- 533 E.D. Bergerova, M. Strasakova, J. Cisar, T. Sopik, M. Dusankova, I. Vincent, J. Klaban, D.  
534 Hanusova, S. Uhercova, L. Hanykova, V. Sedlarik, Impact of solvolysis on the decomposition  
535 efficiency of poly(lactic acid) materials with insight into their non-uniform architecture, Int. J.  
536 Biol. Macromol. 302 (2025) 140529. <https://doi.org/10.1016/J.IJBIOMAC.2025.140529>.
- 537 P. St'ahel, V. Mazánková, D. Podzemná, E. Podzemná, V. Pizúrová, J. Jurmanová, L. Prokeš,  
538 M. Lehocký, K. Ozaltin, H. Pištěková, D. Trunec, Antibacterial Thin Films Deposited from  
539 Propane-Butane Mixture in Atmospheric Pressure Discharge, (2023).  
540 <https://doi.org/10.3390/ijms24021706>.
- 541 D.K. Owens, R.C. Wendt, Estimation of the surface free energy of polymers, J. Appl. Polym.  
542 Sci. 13 (1969) 1741–1747. <https://doi.org/10.1002/APP.1969.070130815>.
- 543 ISO 22196:2011 - Measurement of antibacterial activity on plastics and other non-porous  
544 surfaces, (n.d.). <https://www.iso.org/standard/54431.html> (accessed April 15, 2024).
- 545 J.C.-E. of analytical chemistry, undefined 2000, Interpretation of infrared spectra, a practical  
546 approach, Researchgate.NetJ CoatesEncyclopedia of Analytical Chemistry,  
547 2000•researchgate.Net (n.d.) 10815–10837. <https://www.researchgate.net/profile/Chandana-Chandrasekher/post/How-to-interpret-my-FTIR-spectrum-Is-there-any-online-software-available-to-interpret-the-spectrum/attachment/5ac4a7094cde260d15d6bc94/AS>

- 550 %3A611637941780481%401522837257071/download/joan+coates.pdf (accessed May 2,  
551 2024).
- [552] K. Štěpánková, M. Müllerová, Š. Žídek, H. Pištěková, P. Urbánek, P. Sťahel, D. Trunec, A.  
553 Popelka, N. Kallingal, M. Mozetič, M. Lehocky, Plasma Polymerization of Pentane and  
554 Hexane for Antibacterial and Biocompatible Thin Films, *Plasma Processes and Polymers*  
555 (2025) e2400266. <https://doi.org/10.1002/PPAP.202400266>.
- [556] C. Contini, M.G. Katsikogianni, F.T. O'Neill, M. O'Sullivan, F. Boland, D.P. Dowling, F.J.  
557 Monahan, Storage Stability of an Antioxidant Active Packaging Coated with Citrus Extract  
558 Following a Plasma Jet Pretreatment, *Food Bioproc. Tech.* 7 (2014) 2228–2240.  
559 <https://doi.org/10.1007/S11947-013-1210-9/FIGURES/7>.
- [560] A. Vesel, M. Mozetic, Modification of PET surface by nitrogen plasma treatment, *J. Phys.*  
561 *Conf. Ser.* 100 (2008). <https://doi.org/10.1088/1742-6596/100/1/012027>.
- [562] P.M. Dietrich, S. Bahr, T. Yamamoto, M. Meyer, A. Thissen, Chemical surface analysis on  
563 materials and devices under functional conditions – Environmental photoelectron  
564 spectroscopy as non-destructive tool for routine characterization, *J. Electron Spectros. Relat.*  
565 *Phenomena* 231 (2019) 118–126. <https://doi.org/10.1016/J.ELSPEC.2017.12.007>.
- [566] J.W. Pinder, G.H. Major, D.R. Baer, J. Terry, J.E. Whitten, J. Čechal, J.D. Crossman, A.J.  
567 Lizarbe, S. Jafari, C.D. Easton, J. Baltrusaitis, M.A. van Spronsen, M.R. Linford, Avoiding  
568 common errors in X-ray photoelectron spectroscopy data collection and analysis, and properly  
569 reporting instrument parameters, *Applied Surface Science Advances* 19 (2024) 100534.  
570 <https://doi.org/10.1016/J.APSADV.2023.100534>.
- [572] A. Szczurek, T.N.L. Tran, J. Kubacki, A. Gąsiorek, K. Startek, A. Mazur-Nowacka, R.  
572 Dell'Anna, C. Armellini, S. Varas, A. Carlotto, A. Chiasera, A. Łukowiak, J. Krzak, M.  
573 Ferrari, Polyethylene terephthalate (PET) optical properties deterioration induced by  
574 temperature and protective effect of organically modified SiO<sub>2</sub>–TiO<sub>2</sub> coating, *Mater. Chem.*  
575 *Phys.* 306 (2023) 128016. <https://doi.org/10.1016/J.MATCHEMPHYS.2023.128016>.
- [576] S.M. Pelagade, N.L. Singh, A. Qureshi, R.S. Rane, S. Mukherjee, U.P. Deshpande, V.  
577 Ganesan, T. Shripathi, Investigation of surface properties of Ar-plasma treated polyethylene  
578 terephthalate (PET) films, *Nucl. Instrum. Methods Phys. Res. B* 289 (2012) 34–38.  
579 <https://doi.org/10.1016/J.NIMB.2012.08.010>.

- [530] X. Zhang, L. Wang, E. Levänen, Superhydrophobic surfaces for the reduction of bacterial  
581 adhesion, *RSC Adv.* 3 (2013) 12003–12020. <https://doi.org/10.1039/C3RA40497H>.
- [532] J. Lai, B. Sunderland, J. Xue, S. Yan, W. Zhao, M. Folkard, B.D. Michael, Y. Wang, Study  
583 on hydrophilicity of polymer surfaces improved by plasma treatment, *Appl. Surf. Sci.* 252  
584 (2006) 3375–3379. <https://doi.org/10.1016/J.APSUSC.2005.05.038>.
- [536] E.E. Johnston, B.D. Ratner, Surface characterization of plasma deposited organic thin films, *J.*  
586 *Electron Spectros. Relat. Phenomena* 81 (1996) 303–317. [https://doi.org/10.1016/0368-5872048\(95\)02666-5](https://doi.org/10.1016/0368-5872048(95)02666-5).
- [538] N.Y. Cui, N.M.D. Brown, Modification of the surface properties of a polypropylene (PP) film  
589 using an air dielectric barrier discharge plasma, *Appl. Surf. Sci.* 189 (2002) 31–38.  
590 [https://doi.org/10.1016/S0169-4332\(01\)01035-2](https://doi.org/10.1016/S0169-4332(01)01035-2).
- [539] H. Dvořáková, J. Čech, M. Stupavská, L. Prokeš, J. Jurmanová, V. Buršíková, J. Ráhel, P.  
592 S'ahel, H. Dvořáková, J. Čech, M. Stupavská, L. Prokeš, J. Jurmanová, V. Buršíková, J.  
593 Ráhel, P. S'ahel, Fast Surface Hydrophilization via Atmospheric Pressure Plasma  
594 Polymerization for Biological and Technical Applications, *Polymers* 2019, Vol. 11, 11  
595 (2019). <https://doi.org/10.3390/POLYM11101613>.
- [539] M. Keil, C.S. Rastomjee, A. Rajagopal, H. Sotobayashi, A.M. Bradshaw, C.L.A. Lamont, D.  
597 Gador, C. Buchberger, R. Fink, E. Umbach, Argon plasma-induced modifications at the  
598 surface of polycarbonate thin films, *Appl. Surf. Sci.* 125 (1998) 273–286.  
599 [https://doi.org/10.1016/S0169-4332\(97\)00501-1](https://doi.org/10.1016/S0169-4332(97)00501-1).
- [600] N. Sakudo, D. Mizutani, Y. Ohmura, H. Endo, R. Yoneda, N. Ikenaga, H. Takikawa, Surface  
601 modification of PET film by plasma-based ion implantation, *Nucl. Instrum. Methods Phys.*  
602 *Res. B* 206 (2003) 687–690. [https://doi.org/10.1016/S0168-583X\(03\)00824-3](https://doi.org/10.1016/S0168-583X(03)00824-3).
- [603] M. Toufik, A. Mas, V. Shkinev, A. Nechaev, A. Elharfi, F. Schué, Improvement of  
604 performances of PET track membranes by plasma treatment, *Eur. Polym. J.* 38 (2002) 203–  
605 209. [https://doi.org/10.1016/S0014-3057\(01\)00130-6](https://doi.org/10.1016/S0014-3057(01)00130-6).
- [606] A. Vesel, M. Mozetic, Modification of PET surface by nitrogen plasma treatment, *J. Phys.*  
607 *Conf. Ser.* 100 (2008). <https://doi.org/10.1088/1742-6596/100/1/012027>.
- [608] N. Milaniak, G. Laroche, F. Massines, Atmospheric-pressure plasma-enhanced chemical  
609 vapor deposition of nanocomposite thin films from ethyl lactate and silica nanoparticles,

610 Plasma Processes and Polymers 18 (2021) 2000153.  
611 <https://doi.org/10.1002/PPAP.202000153>.

~~[614]~~ F. Massines, N. Gherardi, N. Naudé, P. Ségur, Recent advances in the understanding of  
613 homogeneous dielectric barrier discharges, *The European Physical Journal Applied Physics*  
614 47 (2009). <https://doi.org/10.1051/EPJAP/2009064>.

~~[615]~~ M. Laurent, E. Desjardins, M. Meichelboeck, N. Naudé, L. Stafford, N. Gherardi, G. Laroche,  
616 M. Laurent, E. Desjardins, M. Meichelboeck, N. Naudé, L. Stafford, N. Gherardi, G. Laroche,  
617 Characterization of argon dielectric barrier discharges applied to ethyl lactate plasma  
618 polymerization, *JPhD* 50 (2017) 475205. <https://doi.org/10.1088/1361-6463/AA916D>.

~~[616]~~ Y. Yuan, M.P. Hays, P.R. Hardwidge, J. Kim, Surface characteristics influencing bacterial  
620 adhesion to polymeric substrates, *RSC Adv.* 7 (2017) 14254–14261.  
621 <https://doi.org/10.1039/C7RA01571B>.

~~[622]~~ Y. Endo, T. Tani, M. Kodama, Antimicrobial activity of tertiary amine covalently bonded to a  
623 polystyrene fiber., *Appl. Environ. Microbiol.* 53 (1987) 2050.  
624 <https://doi.org/10.1128/AEM.53.9.2050-2055.1987>.

~~[625]~~ V. Baidin, T.W. Owens, M.B. Lazarus, D. Kahne, Simple Secondary Amines Inhibit Growth  
626 of Gram-Negative Bacteria through Highly Selective Binding to Phenylalanyl-tRNA  
627 Synthetase, *J. Am. Chem. Soc.* 143 (2021) 623–627.  
628 [https://doi.org/10.1021/JACS.0C11113/ASSET/IMAGES/LARGE/JA0C11113\\_0004.JPEG](https://doi.org/10.1021/JACS.0C11113/ASSET/IMAGES/LARGE/JA0C11113_0004.JPEG).

~~[629]~~ H. Dvořáková, J. Čech, M. Stupavská, L. Prokeš, J. Jurmanová, V. Buršíková, J. Ráhel', P.  
630 St'ahel, Fast Surface Hydrophilization via Atmospheric Pressure Plasma Polymerization for  
631 Biological and Technical Applications, *Polymers* 2019, Vol. 11, Page 1613 11 (2019) 1613.  
632 <https://doi.org/10.3390/POLYM11101613>.

~~[643]~~ R. Mentheour, Z. Machala, Coupled Antibacterial Effects of Plasma-Activated Water and  
634 Pulsed Electric Field, *Front. Phys.* 10 (2022).  
635 <https://doi.org/10.3389/FPHY.2022.895813/FULL>.

~~[646]~~ S. Zheng, M. Bawazir, A. Dhall, H.E. Kim, L. He, J. Heo, G. Hwang, Implication of Surface  
637 Properties, Bacterial Motility, and Hydrodynamic Conditions on Bacterial Surface Sensing  
638 and Their Initial Adhesion, *Front. Bioeng. Biotechnol.* 9 (2021) 643722.  
639 <https://doi.org/10.3389/FBIOE.2021.643722/BIBTEX>.

[40] X. Zhang, L. Wang, E. Levänen, Superhydrophobic surfaces for the reduction of bacterial  
641 adhesion, RSC Adv. 3 (2013) 12003–12020. <https://doi.org/10.1039/C3RA40497H>.

642